

# MEASURING THE SOURCES OF THE INTERGALACTIC IONIZING FLUX<sup>1</sup>

L. L. COWIE,<sup>2</sup> A. J. BARGER,<sup>2,3,4</sup> L. TROUILLE<sup>3</sup>

*Accepted by The Astrophysical Journal*

## ABSTRACT

We use a wide-field (0.9 deg<sup>2</sup>) X-ray sample with optical and GALEX ultraviolet observations to measure the contribution of Active Galactic Nuclei (AGNs) to the ionizing flux as a function of redshift. Our analysis shows that the AGN contribution to the metagalactic ionizing background peaks at around  $z = 2$ . The measured values of the ionizing background from the AGNs are lower than previous estimates and confirm that ionization from AGNs is insufficient to maintain the observed ionization of the intergalactic medium (IGM) at  $z > 3$ . We show that only sources with broad lines in their optical spectra have detectable ionizing flux and that the ionizing flux seen in an AGN is not correlated with its X-ray color. We also use the GALEX observations of the GOODS-N region to place a  $2\sigma$  upper limit of 0.008 on the average ionization fraction  $f_{\nu}(700 \text{ \AA})/f_{\nu}(1500 \text{ \AA})$  for 626 UV selected galaxies in the redshift range  $z = 0.9 - 1.4$ . We then use this limit to estimate an upper bound to the galaxy contribution in the redshift range  $z = 0 - 5$ . If the  $z \sim 1.15$  ionization fraction is appropriate for higher redshift galaxies, then contributions from the galaxy population are also too low to account for the IGM ionization at the highest redshifts ( $z > 4$ ).

*Subject headings:* cosmology: observations — cosmology: diffuse radiation — galaxies: active — galaxies: intergalactic medium

## 1. INTRODUCTION

One of the most important parameters in the cosmological modeling of galaxies and the intergalactic gas is the level of the ionizing radiation in the universe. This is often referred to as the metagalactic ionizing background. The metagalactic ionizing background is usually computed using composite quasar spectra convolved with the quasar luminosity function (e.g., Haardt & Madau 1996; Madau et al. 1999; Haardt & Madau 2001; Meiksin 2005). Although the relative contributions of the galaxy population and the Active Galactic Nucleus (AGN) population are very poorly determined, based on the ionization stages seen in the intergalactic gas, we suspect that AGNs dominate the production below redshifts of about three. At higher redshifts recent estimates suggest that the AGNs are unable to account for the ionizing flux (e.g., Bolton et al. 2005; Meiksin 2005). In this paper we will confirm this result and show that the AGN contribution is even lower than previously calculated.

It is usually assumed that the ionizing flux at these higher redshifts is predominantly produced by galaxies. However, there is very little evidence that enough ionizing photons escape from the galaxies for this to be true. Most measurements for local and  $z = 1$  galaxies have given only upper limits on the escape fractions (Leitherer et al. 1995; Malkan et al. 2003; Siana et al. 2007), as have recent measurements at  $z = 3$  (Giallongo et al. 2002; Inoue et al. 2006; Fernandez-Soto et al. 2003). However, there is some counter evidence for significant escape fractions, though it is unclear how representative these galaxies are of the

general population. Bergvall et al. (2006) claimed a significant escape fraction in the local blue compact galaxy Haro 11. Shapley et al. (2006) detected ionizing fluxes from two  $z = 3$  Lyman Break Galaxies (LBGs), though these measurements were at a much lower level than a previous measurement made by Steidel et al. (2001). Iwata et al. (2008), using a narrow band filter technique, found ionizing radiation in seven  $z > 3$  LBGs and 10  $z > 3$  Lyman alpha emitters out of a sample of 198  $z > 3$  galaxies in the SSA22 field. However, their analysis of the level of contamination by foreground galaxies is quite crude, and it is also possible that at least some of the detections correspond to objects with misidentified redshifts. Paradoxically, Iwata et al. found a highly significant null detection for the object SSA22a-D3, which is the brighter of the two objects for which Shapley et al. (2006) claimed an ionizing flux detection.

Here we use UV images from the Galaxy Evolution Explorer (GALEX) mission (Martin et al. 2005) to measure the actual ionizing fluxes from very large samples of both galaxies and AGNs. As we illustrate in Figure 1, the 1528 Å filter on GALEX samples the ionizing region of the spectrum at  $z = 1$ . The 2371 Å filter samples it at  $z = 2$ . This avoids issues of the calibration of the spectra and also of the selection functions present in the samples used to construct the composite spectra. It is also now recognized that complete samples of AGNs (at least those which are not Compton thick) are most easily obtained with X-ray observations. Barger et al. (2003) and Fontanot et al. (2007) have used X-ray samples to obtain direct limits on very high-redshift ( $z = 3.5 - 6.5$ ) ionizing

<sup>1</sup>Based in part on data obtained at the W. M. Keck Observatory, which is operated as a scientific partnership among the the California Institute of Technology, the University of California, and NASA and was made possible by the generous financial support of the W. M. Keck Foundation.

<sup>2</sup>Institute for Astronomy, University of Hawaii, 2680 Woodlawn Drive, Honolulu, HI 96822.

<sup>3</sup>Department of Astronomy, University of Wisconsin-Madison, 475 North Charter Street, Madison, WI 53706.

<sup>4</sup>Department of Physics and Astronomy, University of Hawaii, 2505 Correa Road, Honolulu, HI 96822.

fluxes.

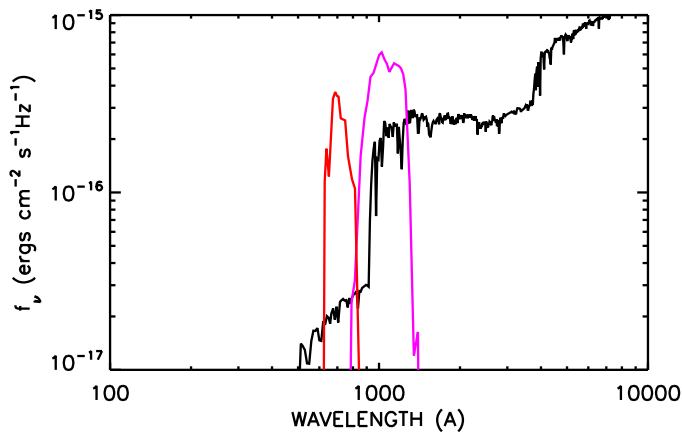


FIG. 1.— The GALEX filter responses plotted for  $z = 1.15$  (colored) and the intrinsic spectrum of a galaxy with a decaying star formation rate (black) having an exponentiation time of  $5 \times 10^9$  yr and an age equal to that of the universe at  $z = 1.15$ . The galaxy model is from Bruzual & Charlot (2003) and does not contain the effects of the galaxy's neutral hydrogen opacity or internal extinction.

In this paper we combine GALEX observations with X-ray samples to determine the ionizing flux from  $z \sim 1$  AGNs and then use this result to estimate the AGN contribution to the metagalactic ionizing background in the redshift range  $z = 0-5$ . We also combine GALEX observations with a large optical galaxy sample with spectroscopic redshifts to determine limits on the escape of ionizing photons at  $z = 1.15$ . We then use this limit to constrain the galaxy contribution in the redshift range  $z = 0-5$ . The structure of the paper is as follows. In §2 we describe our optical and X-ray samples and how we determined the ultraviolet fluxes. In §3 we examine the contribution of optically selected galaxies and X-ray selected AGNs to the ionizing flux. Only the X-ray selected AGNs are positively detected. In §4 we determine how the ionizing flux relates to other properties of the X-ray selected AGNs, showing that the ionizing radiation is only seen in those with broad-lines in their optical spectra. In §5 we examine the evolution of the metagalactic ionizing flux. We show the ionizing fluxes as a function of redshift and compare our results to previous calculations. We summarize our results in §6.

We assume  $\Omega_M = 0.3$ ,  $\Omega_\Lambda = 0.7$ , and  $H_0 = 70 \text{ km s}^{-1} \text{ Mpc}^{-1}$  throughout. All magnitudes are given in the AB magnitude system, where an AB magnitude is defined by  $m_{AB} = -2.5 \log f_\nu - 48.60$ . Here  $f_\nu$  is the flux of the source in units of  $\text{ergs cm}^{-2} \text{ s}^{-1} \text{ Hz}^{-1}$ .

## 2. ULTRAVIOLET FLUXES FOR THE SAMPLES

### 2.1. Optical Sample

We take as our initial optical sample all  $F435W < 26$  galaxies in the  $145 \text{ arcmin}^2$  area of the ACS Great Observatories Origins Deep Survey-North (GOODS-N; Giavalisco et al. 2004) field. The  $F435W$ ,  $F606W$ ,  $F775W$ , and  $F850LP$  magnitudes are taken from the ACS catalogs, the  $U$  magnitudes are from the  $U$ -band images of Capak et al. (2004), and the spectroscopic redshifts are from Barger et al. (2008). Further details and catalogs may be found in Barger et al. (2008).

The GALEX mission obtained a deep 150 ks exposure of the GOODS-N region in early 2004. We measured the near-ultraviolet (NUV;  $2371 \text{ Å}$  central wavelength) and far-ultraviolet (FUV;  $1528 \text{ Å}$  central wavelength) magnitudes at the positions of the optical sample using the GALEX images, which we obtained from the Multimission Archive at STScI (MAST). Given the large point spread function of GALEX ( $4''.5 - 6''$  FWHM), we used an  $8''$  diameter aperture to measure the magnitudes using the GALEX zeropoints of 20.08 for the NUV image and 18.82 for the FUV image from Morrissey et al. (2007). We measured the magnitudes for the brighter objects ( $F435W = 20 - 23.5$ ) in both  $8''$  and  $24''$  diameter apertures and used the median offset of  $-0.41$  between these measurements to correct all of the  $8''$  magnitudes to approximate total magnitudes. The offset is slightly larger than the  $-0.36$  correction from  $7.6''$  diameter magnitudes to total magnitudes determined by Morrissey et al. (2007). The magnitudes agree on average to within 0.05 mag with the SExtractor (Bertin & Arnouts 1996) magnitudes given in the GALEX NUV+FUV merged catalog for the region in the GR4 data release.

We measured the noise level in the images by randomly positioning apertures on blank regions of the sky and measuring the dispersion. (The procedure for selecting the blank regions is outlined in §3.1). We found  $1\sigma$  limits of 26.8 in the NUV image and 27.4 in the FUV image. Of the 6458 galaxies in the  $F435W$  sample, 1017 have  $FUV < 25.5$  and 2528 have  $NUV < 25$  (with considerable overlap between the two).

However, because of the large point-spread function (PSF) of GALEX, contamination by neighbors is a serious problem. This can be dealt with statistically, as we discuss in §3, but it is also of considerable interest to look at the properties of the individual galaxies. We therefore generated a subsample of isolated galaxies where we eliminated any source which was closer than  $8''$  to a source with a brighter GALEX magnitude in the NUV band or where, based on a visual inspection, the position was clearly contaminated by the wings of a nearby bright GALEX source. A substantial fraction of the galaxies in the optical sample are eliminated by this isolation requirement, reducing the effective area to  $48 \text{ arcmin}^2$  based on the fractional number of sources rejected by the isolation criteria. The isolated galaxy sample contains 966 sources with  $NUV < 25$  and 422 sources with  $FUV < 25.5$ . The spectroscopic identifications of these sources are 96% complete to  $NUV = 24.5$  and 98% complete to  $FUV = 25$ .

### 2.2. X-ray Samples

We construct our X-ray samples from the  $2 - 8 \text{ keV}$  sources in the *Chandra* Large Area Synoptic X-ray Survey (CLASXS) of Yang et al. (2004), in the *Chandra* Lockman Area North Survey (CLANS) of Trouille et al. (2008), and within  $8'$  of the pointing center of the 2 Ms *Chandra* Deep Field-North (CDF-N) survey of Alexander et al. (2003). We take as our full X-ray sample the sources with  $f_{2-8 \text{ keV}} > 3.5 \times 10^{-16} \text{ ergs cm}^{-2} \text{ s}^{-1}$  (note that only the CDF-N contributes below  $7 \times 10^{-15} \text{ ergs cm}^{-2} \text{ s}^{-1}$ ). We take as our bright X-ray sample the sources with  $f_{2-8 \text{ keV}} > 7 \times 10^{-15} \text{ ergs cm}^{-2} \text{ s}^{-1}$ . Current tables of redshifts for the full CLASXS, CLANS, and CDF-N X-ray samples are given in Trouille et al. (2008). We define X-

ray AGNs within the sample on energetic grounds as any source more luminous than  $L_X = 10^{42}$  ergs  $s^{-1}$  (Zezas et al. 1998; Moran et al. 1999). Here  $L_X$  is the luminosity calculated in the rest-frame 2 – 8 keV band.

The full X-ray sample contains 662 X-ray sources. Almost all of the sources have been spectroscopically observed and 442 have spectroscopic redshifts. The spectroscopically identified sources should contain a nearly complete sample of all optical broad-line AGNs in the region (Barger et al. 2005; Richards et al. 2005). We find 171 broad-line AGNs, of which 98 have X-ray quasar luminosities ( $L_X > 10^{44}$  ergs  $s^{-1}$ ). The bright X-ray sample with  $f_{2-8 \text{ keV}} > 7 \times 10^{-15}$  ergs  $cm^{-2} s^{-1}$  contains 485 sources, of which 390 have spectroscopic redshifts. Here we have 162 broad-line AGNs, of which 97 have X-ray quasar luminosities.

The CLANS and CLASXS fields are covered by a number of GALEX pointings, all of which are roughly 30 ks in depth, somewhat shorter than the 150 ks CDF-N GALEX exposure. The  $1\sigma$  limits are slightly variable but typically about 26.1 in the NUV images and 26.5 in the FUV images. Only a small fraction (about 4%) of the X-ray sources in the CLANS or CLASXS fields are not covered by one of the GALEX pointings and all of the CDF-N sources are covered. The effective area for the X-ray sources lying within the GALEX pointings is  $0.9 \text{ deg}^2$  at  $f_{2-8 \text{ keV}}$  above  $7 \times 10^{-15}$  ergs  $cm^{-2} s^{-1}$  and  $0.055 \text{ deg}^2$  below.

We measured the GALEX magnitudes for the sources in the X-ray samples which lay within the GALEX pointings in the same way that we measured the GALEX magnitudes for the GOODS-N optical sample. Because the X-ray sources are generally brighter in the FUV than the optical sources, the problem of contamination by galaxies is smaller, and we did not eliminate sources using a separation criterion. (The X-ray sources themselves are so sparse that contamination by another X-ray source may be neglected.) However, we did eliminate four sources where visual inspection showed that there was contamination from a nearby brighter GALEX source at the same wavelength. None of these four sources appear to have any significant FUV flux centered on the object position.

### 2.3. Redshift-Magnitude Relations

In Figure 2 we show redshift versus FUV magnitude for (a) the isolated optical sample with  $FUV < 25$  and (b) the bright X-ray sample with  $FUV < 25$ . In both cases nearly all of the sources are spectroscopically identified, as can be seen from the incompleteness histograms shown at the bottom of each panel. We have redshifts for 323 of the 329 sources with  $FUV < 25$  in the optical sample. Five of the remaining sources could not be identified, and the final source has not been observed. All of the 164 sources with  $FUV < 25$  in the bright X-ray sample have been observed, and only 5 are not identified. In both panels we denote X-ray AGNs by red solid squares, and we enclose X-ray quasars in red large open squares.

At  $z = 0.6$  (dashed horizontal lines in Figure 2) the FUV filter straddles the Lyman break and substantially samples the ionizing radiation (see Fig. 1). As we move to higher redshifts nearly all galaxies vanish from the sample. We can see from Figure 2a that the only source at  $z > 0.7$  in the optical sample with a significant ionizing flux is a broad-line quasar. There is one additional galaxy

at  $z > 0.7$ , but the FUV flux in this object is likely from a nearby  $z = 0.316$  galaxy, which lies  $2.7''$  away. (This source was not eliminated from the sample because the companion is fainter in the NUV band.)

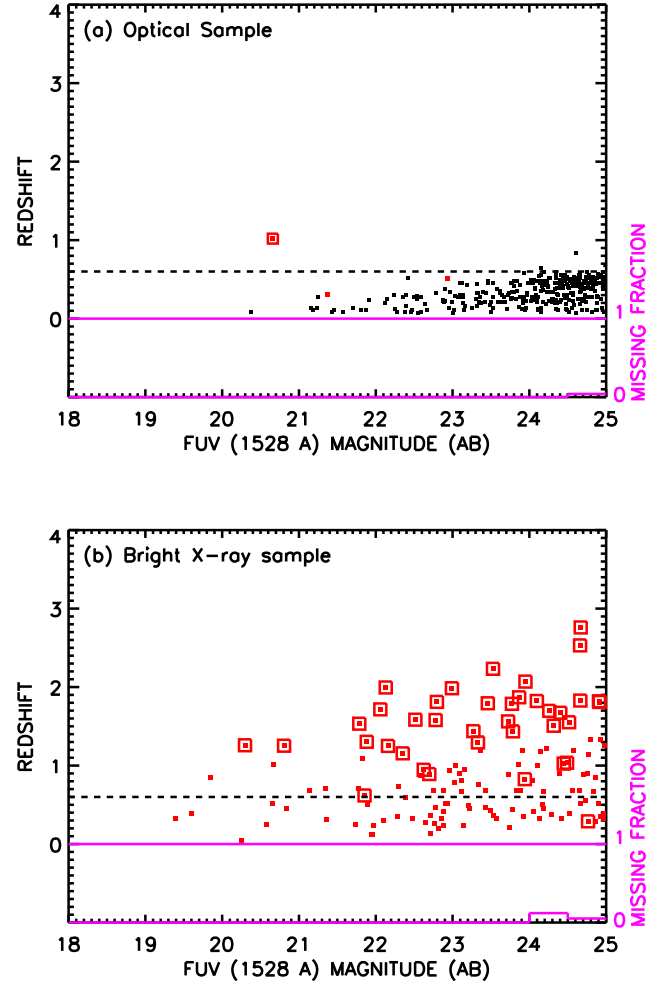


FIG. 2.— Redshift vs. FUV magnitude for (a) the isolated optical sample (GOODS-N) and (b) the bright X-ray sample (X-ray sources in the CLANS, CLASXS, and CDF-N fields with  $f_{2-8 \text{ keV}} > 7 \times 10^{-15}$  ergs  $cm^{-2} s^{-1}$ ). Sources with  $L_X > 10^{42}$  ergs  $s^{-1}$  (X-ray AGNs) are denoted by red solid squares, and those with  $L_X > 10^{44}$  ergs  $s^{-1}$  (X-ray quasars) are shown enclosed in red large open squares. The fraction of spectroscopically unidentified sources per 0.5 mag bin is shown in histogram form at the base of each panel. The  $z = 0.6$  redshift at which the FUV filter straddles the Lyman break is shown by a dashed horizontal line in each panel.

We show this in a different way in Figure 3, where we plot the redshift distributions of all the spectroscopically identified sources in the  $F435W < 24.5$  GOODS-N sample (black histogram) and of only those detected at  $FUV < 25.5$  (blue shading). (The GOODS-N sample is nearly spectroscopically complete to the  $F435W = 24.5$  limit.) We also plot the redshift distributions of all the X-ray AGNs present in the optically selected  $F435W < 24.5$  GOODS-N sample (green histogram) and of only those detected at  $FUV < 25.5$  (red shading). Roughly 76% of the galaxies in this sample below  $z = 0.6$  have  $FUV < 25.5$ . Of the 378 sources in this sample above  $z = 0.7$ , only

four galaxies and two AGNs, including the one galaxy and the one broad-line quasar which we previously noted, have  $FUV < 25.5$ .

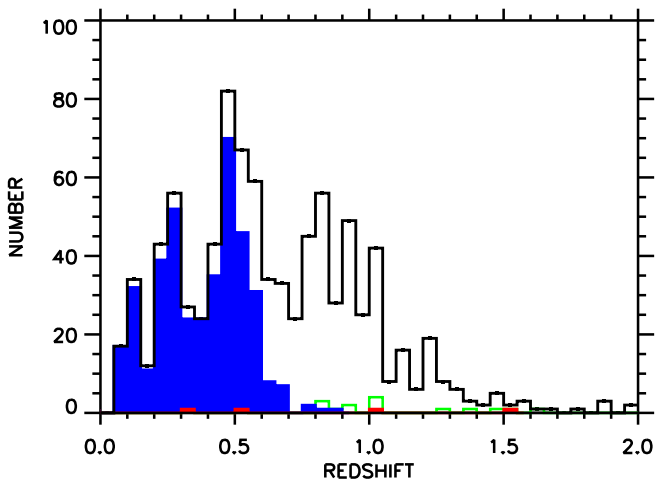


FIG. 3.— The black histogram shows the spectroscopic redshift distribution of the F435W  $< 24.5$  sample in the GOODS-N field. The binning interval is 0.05 in redshift. Galaxies which are detected with FUV magnitudes less than 25.5 are shown with the blue shaded histogram. The green histogram shows the spectroscopic redshift distribution of the X-ray AGNs in this sample. X-ray AGNs which are detected with FUV magnitudes less than 25.5 are shown with the red shaded histogram.

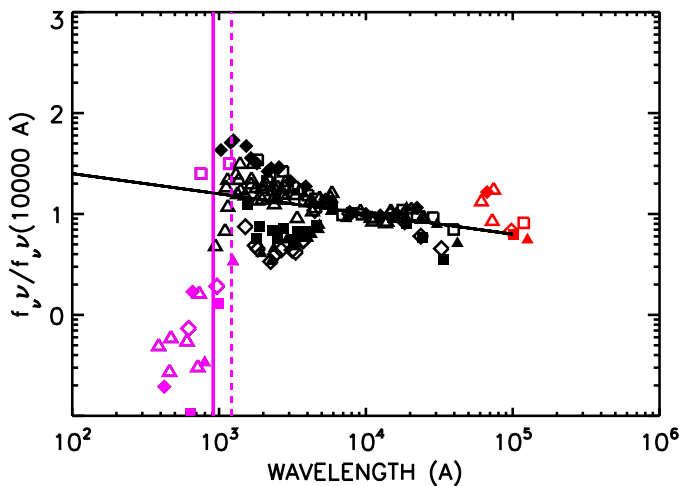


FIG. 4.— Spectral energy distributions of the seven broad-line quasars with  $L_X > 10^{44}$  ergs s $^{-1}$  in the GOODS-N region having redshifts in the range  $z = 0.8 - 3$ . Each quasar is shown with a unique symbol. The GALEX points are shown in purple. The 24  $\mu$ m fluxes are from Treister et al. (2006) and are shown in red. The purple solid line shows the Lyman break, and the purple dashed line shows the position of Ly $\alpha$ . The black solid line shows an  $f_\nu$  vs.  $\nu^{-0.8}$  power law. Only one source has a significant ionizing flux (*open squares*), and it appears to have almost no absorption.

The FUV-bright broad-line quasar is only one of a number of broad-line quasars in the GOODS-N region, and it is immediately clear that these quasars are extremely varied in the number of ionizing photons that we see from them. In Figure 4 we show the spectral energy distributions (SEDs) of the seven broad-line quasars with redshifts between  $z = 0.8$  and  $z = 3$  in the GOODS-N region. Nearly all of the quasars have significant breaks across the

ionization edge, while the one quasar where we see a significant ionizing flux (*open squares*) shows a smooth extension from its longer wavelength SED and almost no opacity to the ionizing photons. A fraction of the breaks will be produced by intervening Lyman Limit Systems (LLS). We quantify this in §4.

The bright X-ray sample in Figure 2b, with its much larger area than the GOODS-N optical sample, contains a significant number of sources with detected ionizing fluxes that we can use to analyze the distribution in properties of the AGN ionizers and their contribution to the ionizing background.

### 3. CONTRIBUTIONS OF OPTICALLY SELECTED GALAXIES AND X-RAY SELECTED AGNS

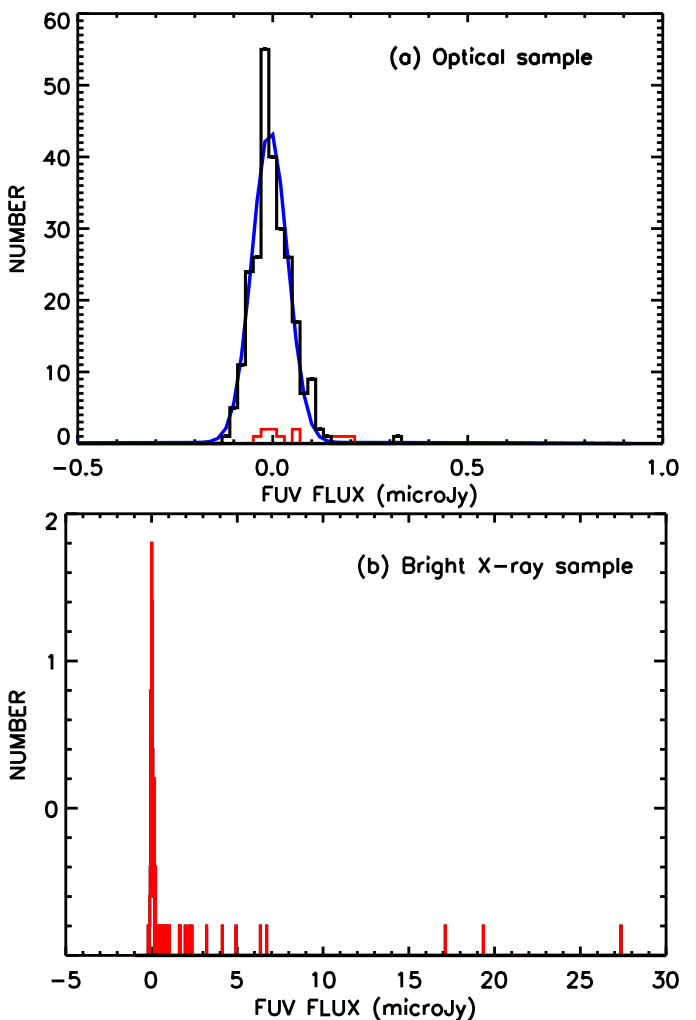


FIG. 5.— (a) Distribution of FUV fluxes in  $\mu$ Jy for the isolated optical sample in the GOODS-N with  $z = 0.9 - 1.4$  (weak or no X-ray emission - *black histogram*; AGNs - *red histogram*). The smooth blue curve shows the distribution of fluxes measured at random positions in the FUV image. All but the one broad-line quasar, which has a 19  $\mu$ Jy flux, are shown in the plot. (b) Same distribution for our bright X-ray sample with  $z = 0.9 - 1.4$  (*red histogram*). Note the much wider x-axis.

In Figure 5a we show the FUV flux distribution of the isolated optical sample in the GOODS-N with  $z = 0.9 - 1.4$ . In Figure 5b we show the FUV flux distribution of the bright X-ray sample with  $z = 0.9 - 1.4$ . The lower redshift cut-off of  $z = 0.9$  places the FUV filter well below the Lyman break. We have chosen a conservative

upper limit on the redshift of  $z = 1.4$  to place the filter well above the drop-off in the intrinsic galaxy spectrum at about  $500 \text{ \AA}$  (see Fig. 1) and to minimize the effects of intervening intergalactic absorption.

### 3.1. Optical Galaxy Sample

In Figure 5a we show the FUV flux distributions of the sources with weak or no X-ray emission (*black histogram*) and of the X-ray AGNs (*red histogram*) in the isolated optical sample in the GOODS-N with  $z = 0.9 - 1.4$ . We overplot the distribution of fluxes measured at random isolated positions in the GOODS-N FUV image (*blue curve*), which matches extremely well to the black histogram. The one detected galaxy in Figure 2a is seen at  $0.3 \mu\text{Jy}$ , but the one detected broad-line quasar is far off the scale of the plot. Excluding only the broad-line quasar while keeping the other X-ray AGNs, these isolated galaxies formally contain a total positive signal of  $3.0 \pm 0.8 \mu\text{Jy}$ . However, when we assess this result we must be concerned about contamination by foreground galaxies and systematic effects of the background subtraction. Indeed, the average FUV flux per galaxy is only  $0.011 \mu\text{Jy}$ , which is considerably below the  $1\sigma$  flux of  $0.039 \mu\text{Jy}$  in the image.

These effects are best tested by Monte-Carlo simulations using random position samples. This also allows us to avoid any subjectivity that might be present in the isolation criteria, since we can analyze analytically selected samples and treat the effects of blending using the simulations. The present problem is also simplified since the contaminating effects primarily arise from the  $z \lesssim 0.6 - 0.7$  galaxies which, as we have seen in Figure 3, are by far the most common class of source with substantial FUV emission. Since we do not expect these to be correlated with the  $z \sim 1$  galaxies of interest, we do not need to be concerned with the effects that might be introduced by correlations, and we can use spatially uniform random samples to determine our backgrounds.

The simplest procedure is to create an analytically selected isolated galaxy sample. To do this we masked  $16''$  radius regions around all  $z = 0 - 0.7$  galaxies and stars with  $\text{FUV} < 23$  and  $8''$  radius regions around all  $z = 0 - 0.7$  galaxies and stars with  $\text{FUV} < 25.5$  and excluded all  $z = 0.9 - 1.4$  galaxies which lay in the masked regions from our sample. In total, we masked regions around 469 galaxies and 14 stars. We also masked  $16''$  radius regions around the four X-ray AGNs in the field with  $\text{FUV} < 25.5$ . These isolation criteria removed 187 galaxies from our initial sample of 680 galaxies with  $z = 0.9 - 1.4$  in the GOODS-N region and reduced the effective area to  $104 \text{ arcmin}^2$ . The average FUV flux per galaxy in the analytic isolated sample is  $0.012 \mu\text{Jy}$ , which is similar to what we found for the smaller isolated sample we constructed in §2.1.

We next created 100 random realizations, each containing the same number of positions as the target sample. We constrained the random positions to lie away from the low-redshift galaxies, stars, and AGNs in the same way that we constrained the target sample. However, since the signal associated with the  $z = 0.9 - 1.4$  galaxies is small, we did not remove or avoid the actual sample when constructing the random samples, but simply generated random  $x$  and  $y$  positions within the unmasked area. From the 100 random realizations we found that a random position sat-

isfying the isolation criteria has an average FUV flux of  $0.018 \mu\text{Jy}$  and a dispersion of  $0.003 \mu\text{Jy}$ . Subtracting this from the average FUV flux per galaxy of  $0.012 \mu\text{Jy}$  measured from the analytic isolated target sample gives an FUV flux of  $-0.006 \pm 0.003 \mu\text{Jy}$  per galaxy.

The average NUV flux per galaxy in the same sample is  $0.44 \mu\text{Jy}$ , while the average  $U$ -band flux per galaxy is  $0.96 \mu\text{Jy}$ . (The corresponding fluxes for a random position at these wavelengths are negligible compared to these values.) The rest-frame wavelengths of the two bands at the midpoint of the  $z = 0.9 - 1.4$  redshift interval are  $1100 \text{ \AA}$  and  $1720 \text{ \AA}$ , respectively. The NUV band straddles the Lyman continuum break in the higher redshift portion of the redshift interval which will reduce the observed flux in this bandpass and it may also be reduced by the Lyman alpha forest (see Fig. 1). We therefore chose to use the  $U$ -band flux as a measure of the rest-frame flux at  $1500 \text{ \AA}$ , assuming a flat  $f_\nu$  SED. We then formed the ratio of the rest-frame  $700 \text{ \AA}$  flux to the rest-frame  $1500 \text{ \AA}$  flux, ignoring the small differential  $K$ -correction as a function of redshift. We call this ratio the ionization fraction to distinguish it from the escape fraction of ionizing photons from the galaxy. Conversion of the ionization fraction to the escape fraction requires knowledge of the intrinsic galaxy spectrum and reddening (e.g., Haardt et al. 1999; Siana et al. 2007). However, for the present purposes of obtaining the ionizing emission of the galaxy population, it is the ionization fraction which is of interest and which we can use to convert the rest-frame UV emission to the ionizing emission. The ionization fraction we obtained using the background-corrected analytic isolated sample is  $-0.006 \pm 0.003$ .

An alternative way to proceed is to subtract the foreground galaxies and stars to form a cleaned image and then to measure the signal associated with the target sample on the cleaned image. This has the virtue of allowing us to measure a larger fraction of the target sample and to avoid using the somewhat arbitrarily sized masking regions selected in the previous procedure. To form a cleaned image we fitted and subtracted all of the  $z < 0.7$  galaxies with  $\text{FUV} < 25.5$  in the GOODS-N from the GALEX image, as well as all of the stars and the four X-ray AGNs with  $\text{FUV} < 25.5$ . As can be seen from Figures 2a and 3, this should remove nearly all of the signal from directly detected objects and therefore minimize the effects of blending and optimize the background subtraction.

Our procedure for this cleaning was to normalize the GALEX PSF, which we determined by stacking the FUV detected stars in the image, to the measured flux of each galaxy and then to subtract this from the image. Most galaxies are very compact compared to the broad GALEX PSF, but to remove the 36 brighter objects with  $\text{FUV} < 22.5$ , which may be more extended, we masked out a  $12''$  region around these galaxies. In our subsequent analysis we exclude objects which fall within these masked regions and correct the area appropriately.

For each subset sample from the full  $\text{F435W} < 26$  sample to be analyzed, we measured the fluxes in the cleaned image at the actual positions of the sample and then created 100 random samples with an equal number of positions as the sample to determine the background and dispersion. We then subtracted this background from the



measured signal of the sample to obtain the true signal. Again, since the signal associated with the  $z = 0.9 - 1.4$  galaxies is small, we did not remove or avoid the actual sample when constructing the random samples.

For the 626 spectroscopically identified  $z = 0.9 - 1.4$  galaxies with  $F435W < 26$  that are not X-ray AGNs and are not in the small masked areas, we find an average background-corrected FUV flux per galaxy of  $-0.005 \pm 0.002 \mu\text{Jy}$ . The average NUV flux per galaxy is  $0.51 \mu\text{Jy}$ , and the average  $U$ -band flux per galaxy is  $0.97 \mu\text{Jy}$ . We note again that the NUV and  $U$  signal associated with a random position is negligible. The inferred ionization fraction is  $-0.006 \pm 0.003$ . This procedure gives a consistent result with the analytic isolation simulations described above. Both give negative fluxes but are consistent with a zero flux at just over the  $2\sigma$  level.

We can also directly compare the distribution of fluxes in the observed target sample with that from the total of all 100 realizations of the random sample to test if they are different from one another. In Figure 6 we compare the cumulative distribution of the FUV fluxes for the  $z = 0.9 - 1.4$   $F435W < 26$  sample measured from the cleaned image (*black curve*) with that measured from the random sample (*red curve*). A Kolmogorov-Smirnov test give a 1% probability that the target sample has the same distribution as the random sample.

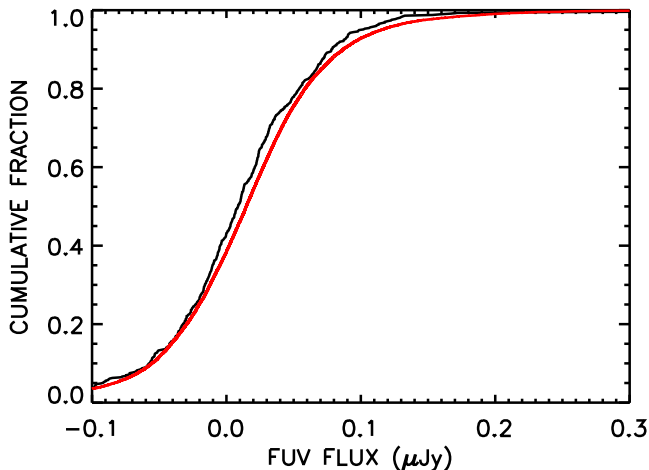


FIG. 6.— Cumulative fraction of sources vs. FUV flux measured in the cleaned image. The black curve shows the  $F435W < 26$  sources in the  $z = 0.9 - 1.4$  redshift interval, and the red curve shows the random sample.

For the nearly spectroscopically complete  $F435W < 24.5$  sample, there are 363  $z = 0.9 - 1.4$  galaxies that are not X-ray AGNs and are not in the small masked areas. Here we find an average background-corrected FUV flux per galaxy of  $-0.005 \pm 0.003 \mu\text{Jy}$ . The average NUV flux per galaxy is  $0.65 \mu\text{Jy}$ , and the average  $U$ -band flux per galaxy is  $1.34 \mu\text{Jy}$ . The inferred ionization fraction is  $-0.005 \pm 0.003$ .

We should probably not take the negative signal too seriously, given its statistical significance in all of the measurements described above. However, the average negative flux may seem worrying at first sight and suggestive of some type of systematic error in the procedure. We

tested this by measuring the signal for the 229 galaxies with  $z > 1.6$  with the analytic isolation procedure. Here we find an average background-corrected FUV flux per galaxy of  $0.001 \pm 0.004 \mu\text{Jy}$ . Thus, the negative signal seems to be associated only with the specific target sample.

However, it is worth noting that the galaxies could have an effective negative signal if their shadowing effect on the ionizing background exceeded their direct emission. The galaxies will block any background light at these wavelengths over the region where their neutral hydrogen column density makes them a LLS. The shadowing effect may extend over a larger area than any FUV emission, making the larger apertures needed for the GALEX observations more sensitive to it. Such shadow galaxies could be used to make a measure of the ionizing flux and of the extent of the neutral hydrogen in the individual galaxy. However, higher spatial resolution observations would be more appropriate for such an analysis than the GALEX data.

In all of our estimates above, systematics could raise the absolute value of the error, though they will not change the ratio of the signal to the error. In particular, we should allow for uncertainties in the extrapolation to form the 1500 Å flux, possible systematic errors in the determination of the FUV fluxes (Morrissey et al. 2007), and uncertainties in the aperture corrections to total magnitudes. Specifically, we include the possibility of a systematic error of 0.2 in the relative FUV and  $U$ -band magnitude determinations, which would raise the error in the ionization fraction to 0.004. Allowing for this level of systematic error and also ignoring the negative signal, we take the  $2\sigma$  limit of 0.008 as our upper limit on the ionization fraction in the  $z \sim 1$  galaxy population in what follows.

Given the relatively small size of the GOODS-N field, we might also be concerned that we are missing the rare FUV-bright galaxies. Since we see no FUV-bright galaxies in the field, we adopt a  $1\sigma$  upper limit of 1.8 such galaxies (Gehrels 1986). Adopting a typical value for the FUV magnitude of 23—comparable to the brightest  $z \sim 0.6$  galaxies (Fig. 2)—one such bright galaxy would correspond to an average contribution of  $0.006 \mu\text{Jy}$  per galaxy from the 680 measured galaxies. This is already smaller than the adopted limit. However, using an FUV magnitude of 23 is in fact extreme, since even young star-forming galaxies will have a strong break across the Lyman edge, so the true contribution will be smaller. It does remain conceptually possible that there may be unique environments where UV ionizing galaxies preferentially form and that we simply have not sampled these with the GOODS-N area. This can only be tested with larger area samples.

In Figure 7a we show the ratio of the rest-frame 700 Å flux to the rest-frame 1500 Å flux (the ionization fraction) as a function of the absolute rest-frame 2000 Å magnitude computed from observed-frame  $F435W$  (*black squares*). Here we use the cleaned FUV images and do the background subtraction as described above. The red line shows the  $2\sigma$  upper limit of 0.008 on the average ionization fraction for the full  $F435W < 26$  sample. In Figure 7b we show the ionization fraction versus observed-frame  $F435W - F850LP$  color (roughly rest-frame 2000 Å – 4200 Å). There is no significant detection as a function of either luminosity or color.

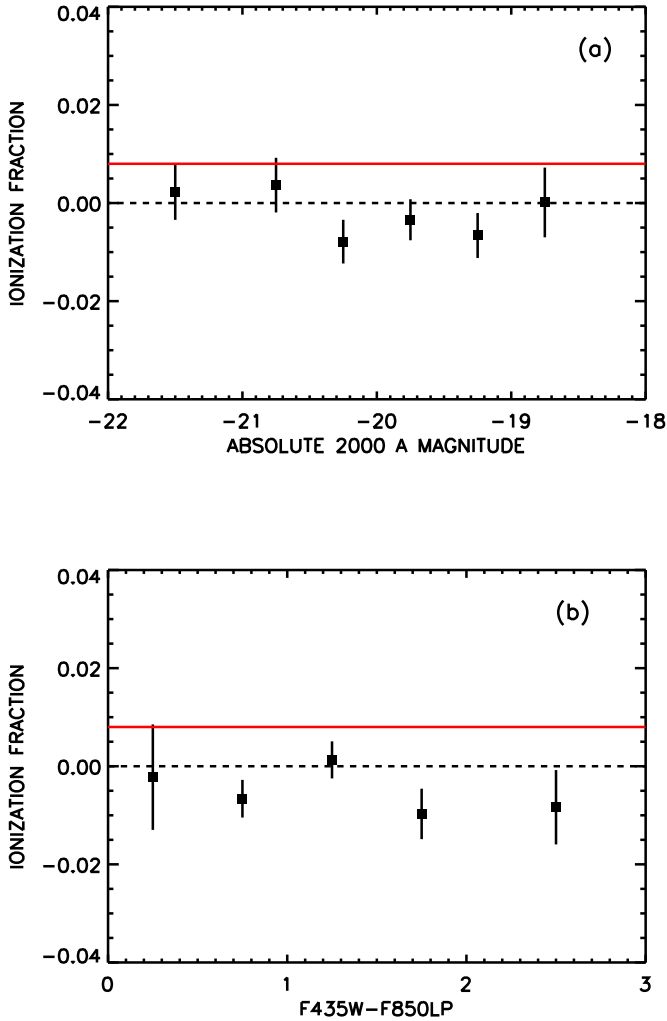


FIG. 7.— (a) Average ionizing fraction (ratio of the rest-frame 700 Å flux to the rest-frame 1500 Å flux) vs. absolute rest-frame 2000 Å magnitude computed from observed-frame F435W. The black squares show the results for the spectroscopically identified  $z = 0.9 - 1.4$  galaxies in the  $F435W < 26$  sample that are not X-ray AGNs. The error bars are  $1\sigma$  statistical errors. The red solid line shows the  $2\sigma$  upper limit of 0.008 on the average ionization fraction for the full sample, including possible systematic errors described in the text. (b) Average ionizing fraction vs. observed frame F435W-F850LP color (roughly rest-frame 2000 Å - 4200 Å) for the  $z = 0.9 - 1.4$  galaxies.

### 3.2. Bright X-ray Sample

The one FUV-bright broad-line quasar in the GOODS-N gives a flux of  $19 \mu\text{Jy}$ , which dominates the signal in the field. We show this in Figure 8, where we compare the summed image formed using our cleaned image of the 626 spectroscopically identified  $z = 0.9 - 1.4$  galaxies in the  $F435W < 26$  sample that are not X-ray AGNs (*left panel*) with the summed image of the 29 GOODS-N X-ray AGNs with  $z = 0.9 - 1.4$  (*right panel*). The clear detection in the FUV sum of the X-ray AGNs is totally dominated by the FUV-bright broad-line quasar. The remaining 28 X-ray AGNs in this redshift interval are consistent with having no ionizing flux. However, given the small number

of contributing broad-line AGNs, we need the much wider field of the bright X-ray sample to accurately compute the AGN contribution to the ionizing flux.

In Figure 5b we show the FUV flux distribution for our bright X-ray sample with  $z = 0.9 - 1.4$  (*red histogram*). 32 sources in this redshift interval have FUV magnitudes brighter than the  $5\sigma$  limit of the image, and the total measured flux is  $112 \mu\text{Jy}$  for the  $0.9 \text{ deg}^2$  area. This result is not affected by our exclusion of the four sources which are contaminated by neighbor galaxies (see §2.2), since, even without any cleaning, these sources only have a total flux of  $2 \mu\text{Jy}$ . We analyzed the background level and variance by again creating random realizations, each containing the same number of positions as the target sample, and measuring at the positions in the raw images. We found the background to be small relative to the signal. The background-corrected signal is  $100 \pm 5 \mu\text{Jy}$ , where the error is the variance in the background determination. This measured signal would correspond to  $4.5 \mu\text{Jy}$  in the small GOODS-N region. Thus, the one FUV-bright broad-line quasar in the GOODS-N region is an anomaly.

Even with the larger area, there are only a small number of AGNs which are seen to have ionizing radiation. The three brightest AGNs produce 60% of the flux, and the seven brightest AGNs produce almost 80%. Given the small number of contributing sources and the peculiar distribution of the fluxes, we have used a jackknife analysis to make a more accurate estimate of the uncertainty in the AGN contribution. This gives a 68% confidence range of  $\pm 33 \mu\text{Jy}$  on the signal. It should be noted that large uncertainty in the jackknife analysis does not mean that the ionizing flux contribution from the AGN is not highly significant. This is properly inferred from the results in the last paragraph. The large uncertainty from the jackknife method is a consequence of the fact that only a small fraction of the X-ray sources which are detected in the FUV dominate the production of ionizing radiation.

We conclude that only the X-ray sources can be detected at ionizing frequencies and that an extremely small number of these dominate the ionizing flux production. The emission per unit comoving volume of the X-ray quasars ( $L_X > 10^{44} \text{ ergs s}^{-1}$ ) is  $\nu\lambda_\nu = (3.4 \pm 1.5) \times 10^{39} \text{ ergs s}^{-1} \text{ Mpc}^{-3}$  at  $z = 1.15$ , where we have used the jackknife method to estimate the uncertainty. Here  $\lambda_\nu$  is the luminosity density per unit frequency, which is the sum of the luminosities per unit frequency of all the objects divided by the cosmological volume that they occupy. We now turn to a more detailed analysis of the contribution from the bright X-ray sample to try to understand the FUV-bright AGNs in more detail.

### 4. IONIZING PROPERTIES OF X-RAY SELECTED AGNS

We can try to refine the results of §3 by considering how the ionizing flux relates to other properties of the AGNs. In Figure 9a we show  $L_\nu\nu(700 \text{ Å})$ , where 700 Å is the rest-frame wavelength, for the  $z = 0.9 - 1.4$  sources in the full X-ray sample versus rest-frame 2 - 8 keV luminosity,  $L_X$ . We divide the sources into those with broad lines (*red squares*) and those without (*black diamonds*). As might be expected, only the broad-line AGNs are ionizers. One of the non-broad-line AGNs is significantly detected, but an inspection of its spectrum shows that it appears to be contaminated by a lower redshift galaxy. Thus, we exclude

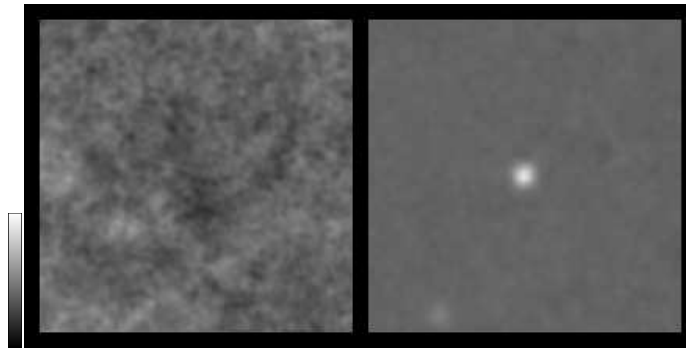


FIG. 8.— Summed image of the 626 spectroscopically identified  $z = 0.9 - 1.4$  galaxies in the  $F435W < 26$  sample that are not X-ray AGNs and do not lie in the small number of masked areas in the cleaned image (*left panel*) and the 29 GOODS-N X-ray AGNs with  $z = 0.9 - 1.4$  (*right panel*). The noise is higher in the galaxy image because of the larger number of objects. The scaling is the same in both images. In each case the image size is  $80''$  on a side, and a positive signal would appear at the center of the image. The strong detection in the right panel is dominated by the one FUV-bright broad-line quasar. There is no detected signal in the left panel.

it from further consideration.

In Figure 9a we use large open squares to show the mean values of  $L_\nu\nu(700 \text{ \AA})$  versus  $L_X$  for the  $z = 0.9 - 1.4$  broad-line AGNs. For all of the  $z = 0.9 - 1.4$  broad-line AGNs together we find a mean ratio of  $L_\nu\nu(700 \text{ \AA})/L_X = 3.95$ . However, there is a very wide spread in the individual ratios. The dominant sources have ratios that are almost an order of magnitude higher than the mean ratio of 3.95. The FUV and optical are more tightly correlated (see Fig. 9b), so a considerable part of the observed spread in Figure 9a comes from the dispersion in the relation of the optical to the X-ray fluxes of the sources (see Fig. 9c). A linear relation with a normalization of 3.95 (*blue dashed line*) does not describe the mean values of  $L_\nu\nu(700 \text{ \AA})$  with  $L_X$  very well. However, a non-linear relation does. The best power law fit to the mean values gives  $L_\nu\nu(700 \text{ \AA})/L_X = 3.53 \times (L_X/10^{44} \text{ ergs s}^{-1})^{0.46}$  with a  $1\sigma$  uncertainty of 0.05 in the power law index (*black solid line*). This non-linear dependence follows from the well-known non-linear dependences of the optical and ultraviolet luminosities of broad-line AGNs on X-ray luminosity (e.g., Vignali et al. 2003a, 2003b; Strateva et al. 2005; Steffen et al. 2006; see Fig 9c).

In Figure 9b we show the dependence of  $L_\nu\nu(700 \text{ \AA})$  on  $L_\nu\nu(2300 \text{ \AA})$  for the  $z = 0.9 - 1.4$  sources in the full X-ray sample, which is tighter. The rest-frame 2300  $\text{\AA}$  luminosity is computed from the  $g$ -band magnitudes obtained on the CFHT Megaprime camera by Trouille et al. (2008). This filter is centered at an observed-frame wavelength of 4900  $\text{\AA}$ . Once again we ignore small differential  $K$ -corrections assuming  $f_\nu$  is flat. We see it is the broad-line AGNs that make up the UV-luminous population. The broad-line AGNs divide about equally into those which are well described by a  $L_\nu \sim \nu^{-1.35}$  power law between the two wavelengths (*green dotted line*) and those which have little or no ionizing flux. We use large open squares to show the mean values of  $L_\nu\nu(700 \text{ \AA})$  versus  $L_\nu\nu(2300 \text{ \AA})$  for the  $z = 0.9 - 1.4$  broad-line AGNs. For all of the  $z = 0.9 - 1.4$  broad-line AGNs together we find a mean ratio of  $\nu L_\nu(700 \text{ \AA})/\nu L_\nu(2300 \text{ \AA}) = 0.47$ . A linear relation with this normalization (*blue dashed line*) provides a reasonable fit to the mean values. In fact, the best power law fit to the mean values (*black line*), which has a power law index of  $0.90 \pm 0.18$ , is consistent with the

linear relation.

We can compare our mean ratio with that of Trammell et al. (2007), who analyzed the GALEX fluxes for a large sample of Sloan Digital Sky Survey (SDSS) quasars. Their quasars are about an order of magnitude higher in luminosity than the present sample, but their mean ratio of  $\nu L_\nu(700 \text{ \AA})/\nu L_\nu(2300 \text{ \AA})$  is similar. Trammell et al. (2007) only included sources with detected FUV magnitudes, for which they find a ratio of about 0.5. Allowing for the roughly one-third of sources which they do not detect, this value could be as low as 0.33. However, given that these two numbers closely bracket our present results, it is clear that there is not a large luminosity dependence in the ratio.

Finally, in Figure 9c we show the well-known non-linear dependence of  $L_\nu\nu(2300 \text{ \AA})$  on  $L_X$ . The best fit power law gives  $\nu L_\nu(2300)/L_X = 7.46 \times (L_X/10^{44} \text{ ergs s}^{-1})^{0.31}$  with a  $1\sigma$  uncertainty of 0.21 in the index (*black line*). This is almost identical to the relation found by Vignali et al. (2003a; see also Richards et al. 2005 for details on converting the Vignali et al. relation into the form used here) (*red dotted line*).

One can next ask if there is any relation between the X-ray properties of the broad-line AGNs and the ionizing photon escape. In Figure 10 we plot the ratio of  $L_\nu\nu(700 \text{ \AA})/L_X$  for  $L_X > 3 \times 10^{43} \text{ ergs s}^{-1}$  sources with redshifts  $z = 0.9 - 1.4$  versus X-ray softness, as measured by the ratio of the 0.5 – 2 keV flux to the 2 – 8 keV flux. We divide the sources into those with broad lines (*red squares*) and those without (*black diamonds*). We can again see that all of the non-broad-line AGNs are UV faint. This immediately tells us that we are not misidentifying sources as non-broad-line AGNs when they are really broad-line AGNs, as one might have expected to happen if the broad lines were not visible spectroscopically due to dilution by the host galaxy (Moran et al. 2002; Severgnini et al. 2003; Cardamone et al. 2007). Barger et al. (2005) make a similar argument based on the presence of nuclei in the broad-line AGNs.



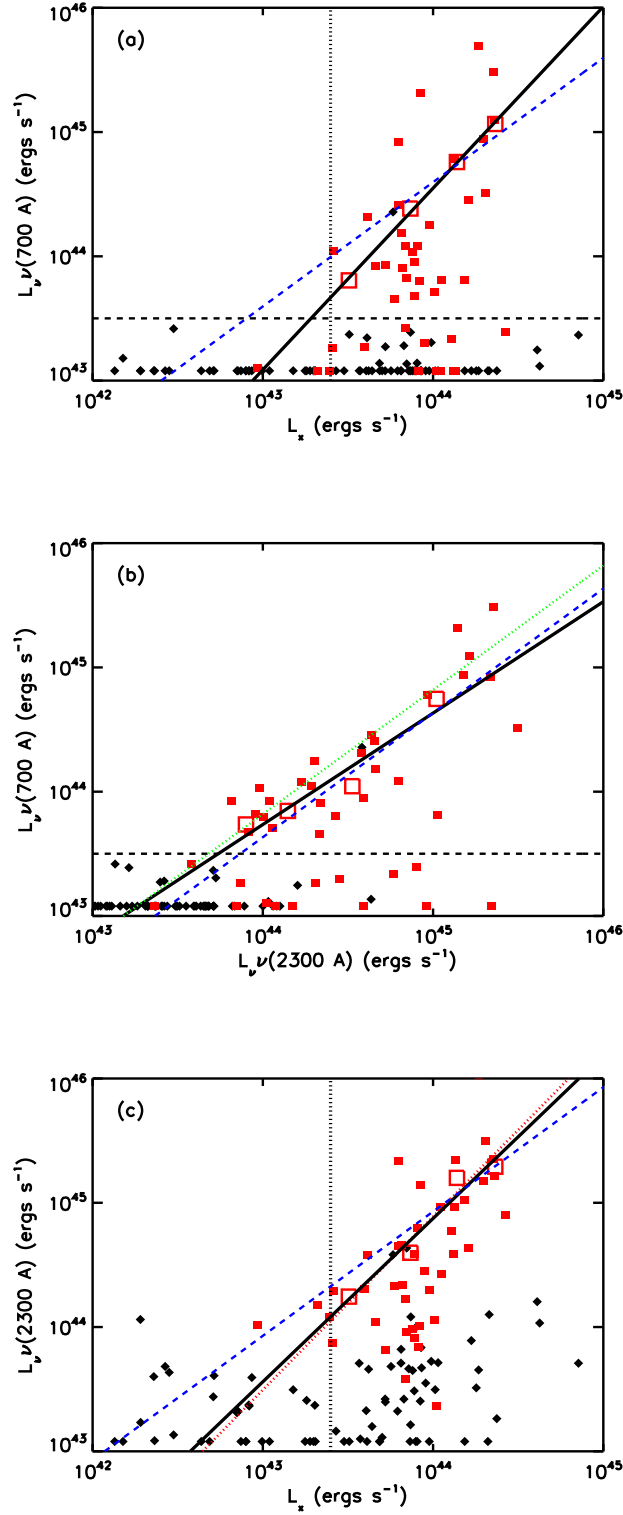


FIG. 9.— The  $z = 0.9 - 1.4$  full X-ray sample (broad-line AGNs - *red solid squares*; non-broad-line AGNs - *black diamonds*; means for the broad-line AGNs - *red open squares*). (a)  $L_\nu\nu$  at rest-frame 700 Å,  $L_\nu\nu(700 \text{ Å})$ , vs. rest-frame 2 – 8 keV luminosity,  $L_X$ . (b)  $L_\nu\nu(700 \text{ Å})$  vs.  $L_\nu\nu(2300 \text{ Å})$ . The green dotted line shows the relation for a source with  $L_\nu \sim \nu^{-1.35}$ . (c)  $L_\nu\nu(2300 \text{ Å})$  vs.  $L_X$ . The red dotted line shows the relation converted from Vignali et al. (2003a). In all three panels we show linear relations (*blue dashed lines*) and best power law fits (*diagonal black lines*) (see text). In (a) and (b) the  $3\sigma$  errors in  $L_\nu\nu(700 \text{ Å})$  for the CLANS and CLASXS fields are shown by the dashed horizontal lines. In (a) and (c) the  $L_X$  above which the field size corresponds to the wide area is shown by vertical dotted lines. Below this the sources are only in the much smaller area of the CDF-N. Sources with low or negative  $y$ -axis values are plotted at a nominal value of  $1.2 \times 10^{43} \text{ ergs s}^{-1}$ . The only non-broad-line AGN with significant  $y$ -axis values in (a) and (b) appears to be contaminated by a lower redshift galaxy (see text).

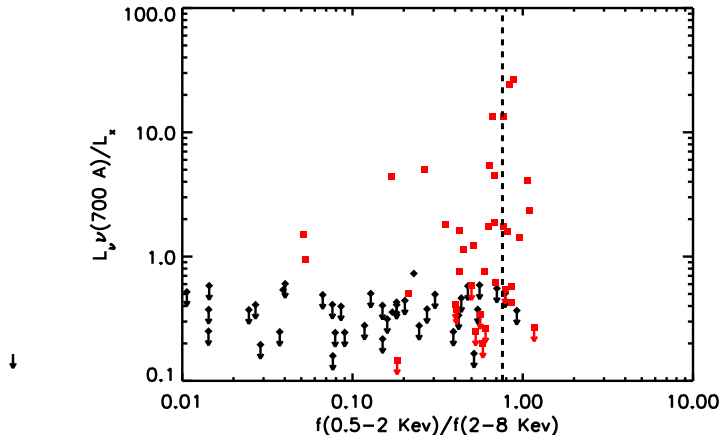


FIG. 10.— Ratio of  $L_{\nu\nu}$  at rest-frame 700 Å,  $L_{\nu\nu}(700 \text{ Å})$ , to rest-frame 2–8 keV luminosity,  $L_X$ , vs. X-ray softness, as measured by the ratio of the 0.5–2 keV flux to the 2–8 keV flux,  $f_{0.5-2 \text{ keV}}/f_{2-8 \text{ keV}}$  for the  $z = 0.9 - 1.4$  redshift range. Only sources with 2–8 keV luminosities above  $3 \times 10^{43} \text{ ergs s}^{-1}$  are shown. Broad-line AGNs are denoted by red squares, and non-broad-line AGNs by black diamonds. The flux ratio for a power law spectrum with photon index  $\Gamma = 1.8$  is shown by the vertical dashed line. Sources with 700 Å fluxes less than  $0.2 \mu\text{Jy}$  are shown with downward pointing arrows.

Indeed, we can pick out a large fraction of the broad-line AGNs simply on the basis of their having a significant FUV flux. Specifically, none of the 45 non-broad-line AGNs with  $L_X > 10^{43} \text{ ergs s}^{-1}$  and redshifts  $z = 0.9 - 1.4$  are detected above the FUV flux limit of  $0.26 \mu\text{Jy}$  ( $3\sigma$ ), while  $70 \pm 14\%$  of the broad-line AGNs are. Thus, the GALEX observations can be used to pick out most of the broad-line AGNs in the X-ray sample. More interestingly, the selection does not seem to depend on the X-ray softness, though the number of X-ray hard broad-line AGNs in the sample is small. As can be seen in Figure 10, we have six broad-line AGNs with 0.5–2 keV to 2–8 keV flux ratios less than 0.3, and four of these have significant FUV detections. There seems to be nothing unusual about the optical spectra of the broad-line AGNs which are detected. Apparently, broad-line AGNs can have a high ratio of the ionizing flux to the X-ray flux, even if the source is quite X-ray hard. This at once says that there is not a one-to-one correspondence between the X-ray spectral index and the neutral hydrogen opacity to the source, since any substantial neutral hydrogen opacity would have the effect of wiping out the ionizing flux, as indeed is invariably seen in the non-broad-line AGNs. A detailed discussion of the comparison between the X-ray and the optical and ultraviolet properties will be given in L. Trouille et al. (2008, in preparation).

Regardless of the interpretation of the results, we conclude that the production of the ionizing flux is best traced by optical spectroscopic broad-line AGN selection, rather than by X-ray or combined X-ray and optical selection, since the X-ray color of the broad-line AGN is not correlated with the presence of the ionizing flux, and non-broad-line AGNs are simply not detected. This considerably simplifies the task of computing the evolution of the metagalactic flux with redshift, since we believe that the

spectroscopic broad-line AGNs are relatively completely identified in the X-ray samples.

The remaining question is why some broad-line AGNs are essentially unobscured in the FUV (we shall refer to these as clear-channel broad-line AGNs), while others with similar luminosities are substantially absorbed in the FUV (we shall refer to these as extinguished broad-line AGNs). A substantial part of the explanation is obscuration by intervening LLSs along the line of sight which, even at  $z = 1$ , is a significant effect. At  $z = 1$  the density of LLS is approximately 0.9 per unit redshift, which would result in about 40% of the sources being obscured (e.g. Storrie-Lombardi et al. 1994). This is very similar to the fraction of sources with weak ionizing flux in the present sample and in Trammell et al. (2007).

However, a detailed analysis shows the situation is slightly more complicated. Storrie-Lombardi et al. (1994) find that Mg II absorption line systems with rest-frame equivalent widths above  $0.3 \text{ Å}$  are a very close proxy for LLS. Thus, we can approach the problem empirically, since we can easily detect such systems in the spectra of our broad-line AGNs.

In Figures 11a and 11b we show the spectral index  $\alpha$  (where  $L_{\nu} \sim \nu^{\alpha}$ ) computed between 700 Å and 2300 Å versus  $L_{\nu\nu}(2300 \text{ Å})$ . In Figure 11a we use the observed FUV flux to compute the rest-frame 700 Å flux, and in Figure 11b we use the observed NUV flux. We do not include the additional  $K$ -correction as a function of redshift relative to the mean redshift, since this would require assumptions about the SED. However, this effect should be small. In Figure 11a we show the broad-line AGNs with  $z = 0.9 - 1.6$  and  $L_{\nu\nu}(2300 \text{ Å}) > 5 \times 10^{44} \text{ ergs s}^{-1}$ . In Figure 11b we show the broad-line AGNs with  $z = 1.9 - 2.5$  and  $L_{\nu\nu}(2300 \text{ Å}) > 2 \times 10^{45} \text{ ergs s}^{-1}$ . Note that the upper redshift limit in the latter is set by the requirement that Mg II at the quasar redshift be on the spectrum. The spectral indices of sources with FUV fluxes below the  $2\sigma$  threshold have been calculated using the  $2\sigma$  threshold and are shown with downward pointing arrows. At lower luminosities the uncertainties in the FUV fluxes become too large to determine accurately the spectral indices. We use red squares to show sources without Mg II absorbers and we use black squares to show sources with Mg II absorbers that are associated with the AGNs. We denote sources with intervening Mg II absorbers along the line of sight by black solid diamonds when the redshift of the system is such that it would substantially quench the FUV light and by black open diamonds when the redshift of the system is such that it only partially covers the wavelengths observed by the FUV filter.

As expected, the presence of an intervening Mg II absorber at a redshift which would substantially quench the FUV light (the black diamonds) guarantees that a source is extinguished. (We take sources with spectral indices less than  $-2$  to be extinguished.) However, two of the clearly extinguished sources in the lower redshift interval (Fig. 11a) do not have Mg II absorbers. In one case the wavelength coverage of the spectrum does not extend to short enough wavelengths to ensure that there is not a LLS along the line of sight that could be significantly extinguishing the flux in the FUV filter. In the other case there is no Mg II absorption, and if the extinction is caused

by a LLS, then it must have weak Mg II absorption. The possible very small fraction of LLS without Mg II absorption is discussed in Storrie-Lombardie et al. (1994) and Steidel & Sargent (1992).

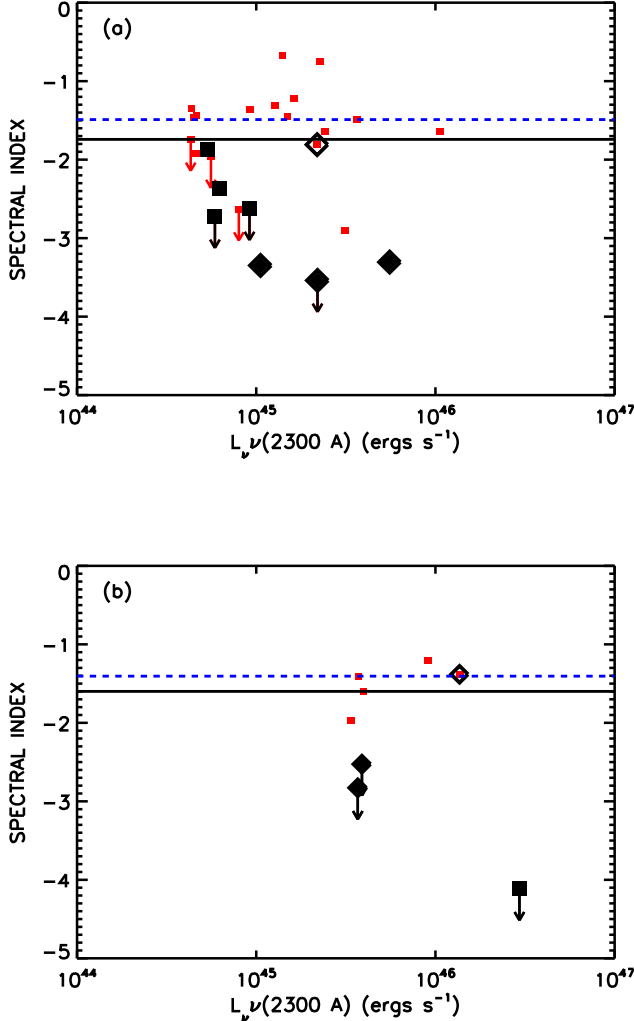


FIG. 11.— (a) Spectral index computed between 700 Å and 2300 Å for  $z = 0.9 - 1.6$  broad-line AGNs with rest-frame 2300 Å luminosities above  $5 \times 10^{44}$  ergs s $^{-1}$  vs.  $L_{\nu}$  at rest-frame 2300 Å,  $L_{\nu}(2300 \text{ Å})$ . Sources with 700 Å fluxes below the  $2\sigma$  threshold are shown at the  $2\sigma$  threshold with downward pointing arrows. Sources without Mg II absorbers in the line of sight are shown with red small squares. Sources with Mg II absorbers associated with the AGNs are shown with black larger squares. Sources with intervening Mg II absorbers along the line of sight are shown with black solid diamonds when the redshift of the system is such that it would substantially quench the FUV light and with black open diamonds when the redshift of the system is such that it would only partially cover the wavelengths observed by the FUV filter. The black line shows the median spectral index for all of the sources. The blue dashed line shows the median spectral index for the sources after removing those with spectral indices less than  $-2$  that do not have Mg II absorbers associated with the AGNs. (b) Same plot for  $z = 1.9 - 2.5$  broad-line AGNs with rest-frame 2300 Å luminosities above  $2 \times 10^{45}$  ergs s $^{-1}$ .

Interestingly, for four of the sources with Mg II absorbers in Figure 11a, the Mg II system is a narrow-line system associated with the AGN (within 10,000 km s $^{-1}$  of the AGN) and is not intervening (*the four black squares*).

In three of the cases the velocity separation is less than 2000 km s $^{-1}$  from the associated AGN. For one other source in Figure 11b (*the black square*) the quasar shows broad absorption features. All of these cases show some level of absorption but in two cases we still see an ionizing flux. Either the conversion of MgII to neutral hydrogen in these systems is different from that of the intergalactic systems or they only partially cover the ionizing region. The actual explanation is not important for the present purposes since there is a critical distinction between associated and intervening systems. In the associated cases the ionizing radiation is absorbed before it emerges into the general intergalactic medium. In contrast, intervening systems are part of the radiative transfer in the intergalactic medium. Thus, in computing the ionizing source term we should not correct for absorption by the associated systems while we should remove the effects of absorption in the intervening systems.

The median spectral index of all of the sources in the lower redshift interval is shown by the black line in Figure 11a and has a value of  $-1.8$  ( $-2.7, -1.4$ ), where the bracketed indices give the 68% confidence range computed using the median sign method. If we remove the three systems with substantial intervening absorption (*three black solid diamonds*) and the two clearly extinguished sources without Mg II absorption (*two red squares*), assuming they are also caused by an intervening LLS, then the median spectral index becomes  $-1.45$  ( $-1.9, -1.2$ ) (*blue dashed line*) and the mean spectral index is  $-1.35$ . The number of sources in the higher redshift interval (Fig. 11b) is small, but the median spectral index after removing the two systems with substantial intervening absorption (*two black solid diamonds*) is consistent with that in the lower redshift interval. Thus, we assume the mean intrinsic spectral index is redshift invariant and adopt the mean value of  $-1.35$  at  $z = 1.15$  in computing the evolution of the metagalactic ionizing flux in §5. Our 700 Å to 2300 Å flux ratio is 0.20, and we scale this to a 912 Å to 2300 Å flux ratio of 0.26, assuming an intrinsic spectrum with an index of  $-1$  below the break, which is similar to that of the broad-line AGNs above the break. This is a factor of 1.5 lower than the value adopted in Haardt & Madau (1996). Using our value in their analysis would bring their results closer to the present values.

## 5. EVOLUTION OF THE METAGALACTIC IONIZING FLUX

The discussion of the previous sections suggests that the best procedure to measure the metagalactic flux is to take the broad-line AGN sample from the X-ray data and to measure its light at NUV wavelengths above the Lyman break. We can then use the average spectral break, corrected for intergalactic absorption, to derive the ionizing flux emissivity. Our broad-line AGN sample chosen from the full X-ray sample probes to much fainter UV magnitudes than the large optical sample and therefore avoids major extrapolations in determining the UV volume emissivity at high redshifts. Using the measured UV fluxes rather than normalizing to the X-ray fluxes avoids the scatter and non-linearity in the relation of the UV to the X-ray. Finally, measuring the flux at the longer wavelengths and then correcting to the ionizing flux avoids the complex problem of correcting for the intervening intergalactic absorption, though at the expense of assuming

a redshift invariant average spectrum for the broad-line AGNs.

In Figure 12 we show the evolution of the comoving volume emissivity determined in this way from the broad-line AGNs in the CLANS, CLASXS and CDF-N fields (*red squares*). We first computed the rest-frame 2300 Å emissivity for our broad-line AGNs in each redshift interval. To determine the rest-frame 2300 Å flux, we interpolated (or extrapolated at the the highest redshifts) using the NUV magnitudes and the  $g$  (observed frame 4900 Å) and  $i$  (observed-frame 7900 Å) magnitudes from Trouille et al. (2008). We then scaled the 2300 Å emissivity to the ionizing volume emissivity using the results from §4. The errors were again computed with the jackknife method. In order to test the completeness, we computed the results as a function of the limiting X-ray flux. Below  $z = 2.5$  the results are dominated by sources with X-ray fluxes above  $7 \times 10^{-15}$  ergs cm $^{-2}$  s $^{-1}$ , which are sampled by the larger area. Above this redshift the results are dominated by sources in the smaller CDF-N area and cosmic variance could be a more significant issue. However, the results substantially converge at fluxes well above the limiting flux in the CDF-N sample. We do not detect any broad-line AGNs above  $z = 4$ , implying a large fall-off in the ionizing fluxes above  $z = 4$ . The evolution of our comoving volume emissivity can be parameterized by the equation

$$\lambda_{ion} = (1.67 + 15.91z - 3.660z^2)10^{23} \text{ ergs s}^{-1} \text{ Hz}^{-1} \text{ Mpc}^{-3}, \quad (1)$$

which is shown as the solid red curve in Figure 12.

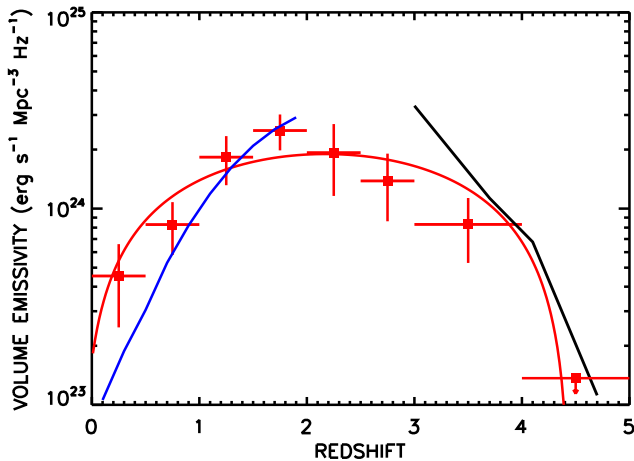


FIG. 12.— Redshift evolution of the comoving volume emissivity of the ionizing flux just below the Lyman continuum edge from broad-line AGNs. The red squares show the values calculated directly from the broad-line AGNs in the full X-ray sample (see text). The error bars are  $1\sigma$  calculated using the jackknife method. There are no broad-line AGNs above  $z = 4$  in our sample, and we show the upper limit based on assuming a one sigma upper limit of 1.8 sources (Gehrels 1986) with the characteristic break luminosity shown in Figure 13b. The blue curve was calculated from the maximum likelihood fit to the Richards et al. (2005) optically selected broad-line AGN sample. We show this only over its valid redshift range. The black solid curve shows the source function computed by Meiksin (2005), which was estimated from the SDSS survey data for broad-line AGNs combined with lower luminosity broad-line AGN constraints from an optical survey at  $z = 3$ . We have corrected this to the presently derived spectral shapes.

In the above calculation we have worked directly with the 2300 Å emissivities determined from the broad-line AGN sample in the CLANS, CLASXS, and CDF-N fields. A similar result can be derived from broad-line AGN X-ray luminosity functions determined as a function of redshift (e.g., Yenko et al. 2008 and references therein), but this would require the use of the more uncertain conversion from X-ray emissivity to ionizing emissivity.

We can also determine the results from the luminosity functions of optically selected samples of broad-line AGNs, where these are deep enough. Here we have computed the comoving ionizing volume emissivity of the broad-line AGNs from the maximum likelihood fit to the Richards et al. (2005) optically selected sample (*blue curve*). As would be expected from the fact that Richards et al. (2005) found their luminosity functions to be in almost perfect agreement with the X-ray luminosity functions, the results derived from the optical and X-ray samples are in extremely good agreement over  $z = 0 - 2$ , where the optical samples are sufficiently deep to make this comparison. It is much harder to use the existing wide-field optically selected samples of broad-line AGNs to make such a comparison at high redshifts, since such samples are not deep enough to probe the dominant contributors. Extrapolations outside the range for which a fit has been derived can produce wildly inaccurate results as discussed by for example Richards et al. (2006).

Meiksin (2005) used the SDSS observations of broad-line AGNs together with the lower luminosity broad-line AGN constraints from the optical survey of Steidel et al. (2002) and Hunt et al. (2004) at  $z = 3$  to estimate the higher redshift values from the optical samples. We show his results with the black solid curve. (We have modified the Meiksin 2005 result which assumed a slightly different value of the break across the Lyman edge to the presently derived spectral shape.) Given the extrapolation uncertainties in this type of estimate, the agreement is quite good. As is well known, the results of Haardt & Madau (1996) and Madau et al. (1999) are too high because of the assumed quasar luminosity functions. However, the present results are considerably lower than even the modified Haardt-Madau values that are often used (e.g., Haardt & Madau 2001; Bolton et al. 2005).

As we have discussed, the production of the ionizing flux is dominated by a small number of sources. We can investigate this directly using the present X-ray selected sample. Typically 3 – 10 sources produce most of the flux in our line of sight in the redshift intervals of Figure 12, even with a 1 deg $^2$  area. (Different lines of sight would see different AGNs as being broad-line and having significant ionizing flux because of the geometric effects of the intrinsic absorption in the AGNs. However, the bulk of the luminous X-ray sources are broad-line AGNs [e.g., Steffen et al. 2003; Barger et al. 2005], and so we expect this effect to be small.) We quantify the number of contributors in Figure 13a, where we show the number density of sources producing 67% of the observed ionizing flux. The number density drops from a value of  $10^{-5}$  Mpc $^{-3}$  at low redshifts, where lower luminosity sources dominate, to about  $10^{-6}$  Mpc $^{-3}$  at  $z = 3.5$ . In Figure 13b we show the luminosity range that produces from 25 – 75% of the ionizing flux. This emphasizes that a rather narrow range of luminosities straddling the break luminosity in the lu-



minosity function produces most of the flux. The typical luminosity of the dominant sources rises quite rapidly at low redshifts, reflecting the rapid nearly pure luminosity evolution of the optical and X-ray luminosity functions in this redshift range (e.g., Barger et al. 2005; Richards et al. 2005). It then reaches a fairly invariant characteristic luminosity of about  $7 \times 10^{29}$  ergs s $^{-1}$  Hz $^{-1}$  above this redshift. This corresponds to an absolute rest-frame magnitude at 2300 Å of  $M_{2300} = -24.5$ .

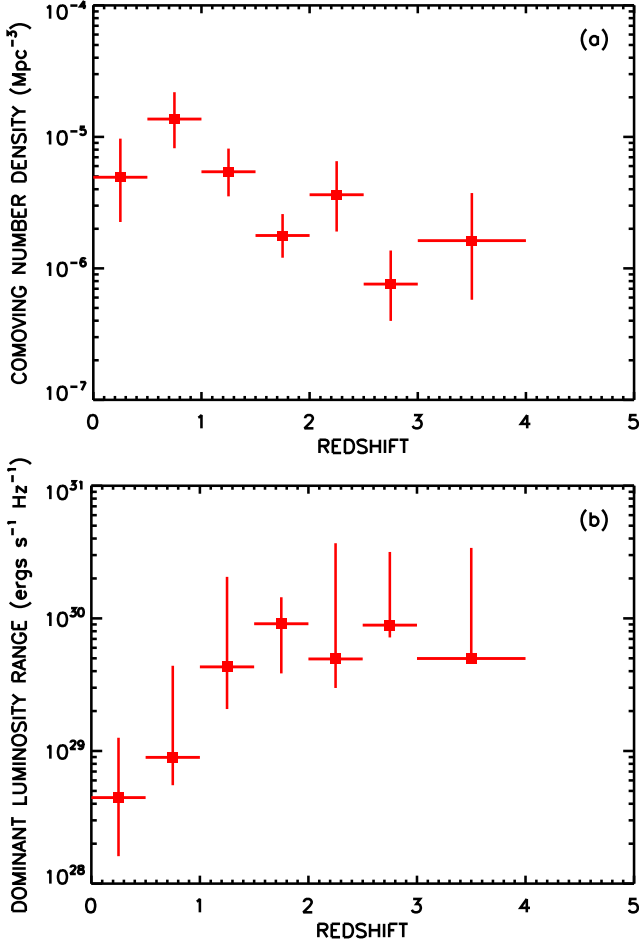


FIG. 13.— (a) Redshift evolution of the comoving volume density of the sources producing 67% of the ionizing volume emissivity. The  $1\sigma$  error bars have been computed using the median sign method. The number of dominant sources in each redshift interval ranges from 3 to 10. (b) The luminosity range of the sources dominating the ionizing volume emissivity. The squares show the luminosity above which 50% of the emissivity is produced, and the vertical lines show the 25% to 75% range.

As pointed out by Madau et al. (1999), the measured absorption distance for the ionizing photons at  $z \sim 3$  is quite small so that the ionization rate is only determined by local sources. They estimate an absorption distance corresponding to  $\Delta z = 2.8(1+z)^{-2}$  at these redshifts, which is  $\Delta z = 0.18$  at  $z = 3$ . Combining this with the comoving number density in Figure 13 gives a contributing number of quasars of about 3000 at  $z = 3$  and 200 at  $z = 4$  in any given region. Beyond this the numbers drop rapidly, and at  $z = 4.5$  there would be less than 20 dominant quasars. We may compare this with Meiksin & White (2003), who self-consistently estimated the absorption distance by normalizing the modeled quasars to

match the required ionization in the Ly $\alpha$  forest and then computing the absorption distance, rather than obtaining it from observations. The number of contributing quasars is higher by factors of several, as would be expected since the present AGN emissivity is too low to account for the ionization at these redshifts. As the number of contributing quasars drops, fluctuations become important, and the contribution of the AGNs to producing transmission in the AGNs is further reduced, increasing the deficiency of these sources for ionizing the IGM (Meiksin & White 2003).

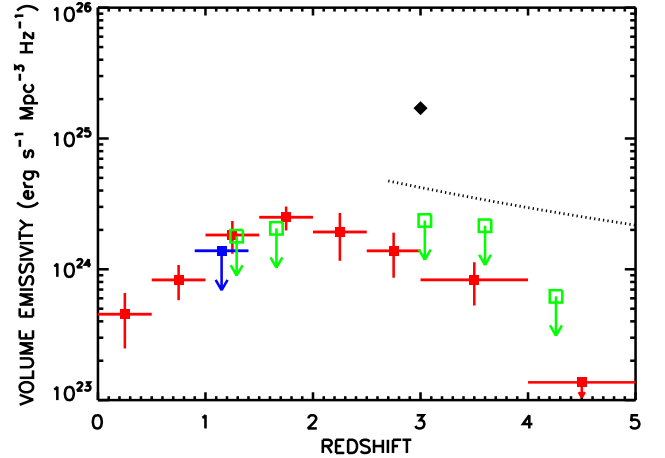


FIG. 14.— Redshift evolution of the comoving volume emissivity of the ionizing flux just below the Lyman continuum break calculated from the broad-line AGNs in the full X-ray sample (red squares) compared with the upper limits for galaxies (blue and green squares). The blue solid square shows our directly measured  $2\sigma$  limit at  $z = 1.15$ . The green open squares show the  $2\sigma$  limits obtained by converting the 1500 Å comoving emissivities from Tresse et al. (2007) to the ionizing emissivities using our  $2\sigma$  upper limit on the average ionization fraction at  $z = 1.15$  (see §3.1) and then multiplying by 1.26 to correct from 700 Å to 912 Å. The black diamond shows the measured value from Shapley et al. (2006)'s LBGs. The dotted line shows the required emissivity to reproduce the Ly $\alpha$  forest structure in the IGM estimated by Meiksin (2005).

In Figure 14 we compare the comoving volume emissivity of the ionizing light just below the Lyman continuum edge calculated from the broad-line AGNs in the full X-ray sample (red squares) with the upper limits for galaxies (blue and green squares). At  $z = 1.15$  we show the directly measured  $2\sigma$  upper limit from the present work as the blue square with the downward pointing arrow. To compute the limits at higher redshifts, we converted the 1500 Å comoving emissivities from Tresse et al. (2007) to the ionizing emissivities using our  $2\sigma$  upper limit on the average ionization fraction at  $z = 1.15$  (see §3.1) and then multiplied by 1.26 to correct from 700 Å to 912 Å. For the highest redshift points ( $z \gtrsim 3$ ) we used the unweighted estimated values from Tresse et al. (2007)'s Table 4. We show these limits on the comoving ionizing emissivity derived from the Tresse et al. (2007) data as green open squares with downward pointing arrows in Figure 14. The Tresse et al. (2007) 1500 Å emissivities are broadly consistent with previous measurements (Steidel et al. 1999; Gabasch et al. 2004; Arnouts et al. 2005; Sawicki & Thompson 2006) and with the present work. The black dotted curve in Figure 14 shows the the required emissivity to reproduce



the Ly $\alpha$  forest structure in the intergalactic medium at  $z > 3$  estimated by Meiksin (2005). We have used the value allowing for reprocessing of the ionizing radiation in the IGM (the dashed curve of Meiksin's Figure 1).

If the high-redshift ionization fraction is as low as our measured limit at  $z = 1.15$ , then the upper limit on the galaxy contribution is slightly low compared with the required ionization. This result is marginal in the  $z = 3 - 4$  range but stronger above  $z = 4$ . However, given the rapid change in the morphologies of the galaxy population beyond  $z = 1$ , we may question whether the  $z = 1.15$  ionization fraction of the present work is applicable to the higher redshift population. If the ionization fraction rises to that measured by Shapley et al. (2006) from their small sample of LBGs, then the galaxy contribution at high redshifts, as shown by the black diamond at  $z = 3$ , would easily match (or indeed exceed) the required ionization. (We note that if Iwata et al. [2008] are correct in their null detection of the brighter of the two Shapley et al. [2006] LBG detections, then the Shapley et al. point would fall by a factor of roughly 3.) However, the Shapley et al. (2006) sample may be biased towards the LBGs that are most likely to have ionizing flux and thus may really be an upper limit even on the LBG contribution. It is therefore critical to understand whether the current measurements of the  $z \sim 3$  LBGs are representative of the population as a whole at these redshifts. The narrow-band ionizing flux surveys of  $z \sim 3$  LBGs currently being worked on by several groups should resolve this question.

## 6. SUMMARY

We have used X-ray, optical, and GALEX observations to measure the contribution of AGNs to the ionizing flux as a function of redshift. Our analysis of a large population of X-ray sources confirms that the AGN contribution to the ionizing flux peaks at around  $z = 2$  and drops rapidly at higher redshifts. It is insufficient to account for

the observationally inferred ionizing flux at high redshifts ( $z > 3$ ). We have also obtained a strong upper limit on the contribution of galaxies to the ionizing flux at  $z = 1.15$  using GALEX observations of a very large sample of rest-frame UV selected galaxies in the GOODS-N region. Our  $2\sigma$  upper limit on the ionization fraction for this population,  $f_{\nu}(700 \text{ \AA})/f_{\nu}(1500 \text{ \AA}) = 0.008$ , yields an upper limit on the comoving ionizing emissivity from the galaxies at  $z = 1.15$ , which is at most comparable to that for the AGNs at  $z = 1.15$ . We briefly discuss the possibility that the galaxies may in fact be net absorbers at these redshifts.

If galaxies are to contribute significantly to the ionizing radiation, then the ionization fraction must increase at higher redshifts. Shapley et al. (2006)'s measured value from their small sample of LBGs at  $z = 3$  is about six times higher than the value from our  $2\sigma$  upper limit on the ionization fraction at  $z = 1.15$ . However, the Shapley et al. (2006) value would be reduced by about a factor of three if the object which is not confirmed by Iwata et al. (2008) is removed. If these LBGs are representative of the high-redshift population as a whole, then this would be adequate to produce the high-redshift ionizing flux. However, it would require an increase in the escape of the ionizing photons from the galaxies as a function of increasing redshift.

We thank the anonymous referee for comments that substantially improved the manuscript. We thank Dan Vandenberg and Avery Meiksin for helpful discussions. We gratefully acknowledge support from NSF grants AST-0407374 and AST-0709356 (L. L. C.) and AST-0239425 and AST-0708793 (A. J. B.), the University of Wisconsin Research Committee with funds granted by the Wisconsin Alumni Research Foundation, and the David and Lucile Packard Foundation (A. J. B.). L. T. was supported by an NSF Graduate Fellowship.

## REFERENCES

- Alexander, D. M., et al. 2003, *AJ*, 126, 539  
 Arnouts, S., et al. 2005, *ApJ*, 619, L43  
 Barger, A. J., Cowie, L. L., Capak, P., Alexander, D. M., Bauer, F. E., Brandt, W. N., Garmire, G. P., & Hornschemeier, A. E. 2003, *ApJ*, 584, L61  
 Barger, A. J., Cowie, L. L., Mushotzky, R. F., Yang, Y., Wang, W.-H., Steffen, A. T., & Capak, P. 2005, *AJ*, 129, 578  
 Barger, A. J., Cowie, L. L., & Wang, W.-H. 2008, *ApJ*, *in press*  
 Bergvall, N., Zackrisson, E., Andersson, F435W.-G., Arnberg, D., Masegosa, J., & Ostlin, G. 2006, *A&A*, 448, 513  
 Bertin, E., & Arnouts, S. 1996, *A&AS*, 117, 393  
 Bolton, J. S., Haehnelt, M., Viel, M., & Springel, V. 2005, *MNRAS*, 307, 1178  
 Bruzual, G., & Charlot, S. 2003, *MNRAS*, 344, 1000  
 Capak, P., et al. 2004, *AJ*, 127, 180  
 Cardamone, C. N., Moran, E. C., & Kay, L. E. 2007, *AJ*, 134, 1263  
 Fernandez-Soto, A., Lanzetta, K. M., & Chen, H.-W. 2003, *MNRAS*, 342, 1215  
 Fontanot, F., Cristiani, S., Monaco, P., Nonino, M., Vanzella, E., Brandt, W. N., Grazian, A., & Mao, J. 2007, *A&A*, 461, 39  
 Gabasch, A., et al. 2004, *A&A*, 421, 41  
 Gehrels, N. 1986, *ApJ*, 303, 336  
 Giallongo, E., Cristiani, S., D'Odorico, S., & Fontana, A. 2002, *ApJ*, 568, L9  
 Giavalisco, M., et al. 2004, *ApJ*, 600, L93  
 Haardt, F., & Madau, P. 1996, *ApJ*, 461, 20  
 Haardt, F., & Madau, P. 2001, in *Clusters and the High Redshift Universe Observed in X-rays*, ed. D. M. Neumann, & J. T. T. Van, (astro-ph/0106018)  
 Hunt, M. P., Steidel, C. S., Adelberger, K., & Shapley, A. 2004, *ApJ*, 605, 625  
 Inoue, A. K., Iwata, I., & Deharveng, J.-M. 2006, *MNRAS*, 371, L1  
 Iwata, I., et al. 2008, *ApJ*, *submitted* (arXiv.0805.4012)  
 Leitherer, C., Ferguson, H. C., Heckman, T. M., & Lowenthal, J. D. 1995, *ApJ*, 454, L19  
 Madau, P., Haardt, F., & Rees, M. J. 1999, *ApJ*, 514, 648  
 Malkan, M., Webb, W., & Konopacky, Q. 2003, *ApJ*, 598, 878  
 Martin, D. C., et al. 2005, *ApJ*, 619, L1  
 Meiksin, A. 2005, *MNRAS*, 356, 596  
 Meiksin, A., & White, M. 2003, *MNRAS*, 342, 1205  
 Moran, E. C., Filippenko, A. V., & Chornock, R. 2002, *ApJ*, 579, L71  
 Moran, E. C., Lehnert, M. D., & Helfand, D. J. 1999, *ApJ*, 526, 649  
 Morrissey, P., et al. 2007, *ApJS*, 173, 682  
 Richards, G. T., et al. 2005, *MNRAS*, 360, 839  
 Richards, G. T., et al. 2006, *AJ*, 131, 2766  
 Severgnini, P., et al. 2003, *A&A*, 406, 483  
 Shapley, A., Steidel, C. C., Pettini, M., & Erb, D. 2006, *ApJ*, 651, 688  
 Siana, B., et al. 2007, *ApJ*, 668, 62  
 Steffen, A. T., Barger, A. J., Cowie, L. L., Mushotzky, R. F., & Yang, Y. 2003, *ApJ*, 596, 23  
 Steffen, A. T., Strateva, I., Brandt, W. N., Alexander, D. M., Koekemoer, A. M., Lehmer, F435W. D., Schneider, D. P., & Vignali, C. 2006, *AJ*, 131, 2826  
 Steidel, C. C., Adelberger, K. L., Giavalisco, M., Dickinson, M., & Pettini, M. 1999, *ApJ*, 519, 1  
 Steidel, C. C., Hunt, M. P., Shapley, A. E., Adelberger, K. L., Pettini, M., Dickinson, M., & Giavalisco, M. 2002, *ApJ*, 576, 653  
 Steidel, C. C., Pettini, M., & Adelberger, K. L. 2001, *ApJ*, 546, 665  
 Steidel, C. C., & Sargent, W. L. W. 1992, *ApJS*, 80, 1

- Storrie-Lombardi, L. J., McMahon, R. G., Irwin, M. J., & Hazard, C. 1994, *ApJ*, 427, L13
- Strateva, I. V., Brandt, W. N., Schneider, D. P., Vanden Berk, D. G., & Vignali, C. 2005, *AJ*, 130, 387
- Sawicki, M., & Thompson, D. 2006, *ApJ*, 642, 653
- Trammell, G. B., Vanden Berk, D. E., Schneider, D. P., Richards, G. T., Hall, P. B., Anderson, S. F., & Brinkmann, J. 2007, *AJ*, 133, 1780
- Treister, E., et al. 2006, *ApJ*, 640, 603
- Tresse, L., et al. 2007, *A&A*, 472, 403
- Trouille, L., Barger, A. J., Cowie, L. L., Yang, Y., & Mushotzky, R. F. 2008, *ApJS*, 179, 1
- Vignali, C., Brandt, W. N., & Schneider, D. P. 2003a, *AJ*, 125, 433
- Vignali, C., et al. 2003b, *AJ*, 125, 2876
- Yang, Y., Mushotzky, R. F., Steffen, A. T., Barger, A. J., & Cowie, L. L. 2004, *AJ*, 128, 1501
- Yencho, B., Barger, A. J., Trouille, L., & Winter, L. M. 2008, *ApJ*, *submitted*
- Zezas, A. L., Georgantopoulos, I., & Ward, M. J. 1998, *MNRAS*, 301, 915